Journal of Advances in Science and Engineering 4 (2021) 1 – 12

Journal of Advances in Science and Engineering (JASE)

Journal homepage: www.sciengtexopen.org/index.php/jase

Numerical analysis of steel columns subject to eccentric loadings

Emmanuel Ufuah

Department of Civil Engineering, Ambrose Alli University, Ekpoma, Nigeria

ARTICLE INFO

Article history:

Received 22 October 2020

Received in revised form
30 November 2020

Accepted 16 December 2020

Available online
21 December 2020

Keywords:

Compressive actions

Critical buckling load

Eccentric loadings

Finite element

Modelling

Steel columns

ABSTRACT

Buckling of framed and plated structures has been a great concern that researchers try to handle over the past decades. In most developing nations such as ours, fewer or no experimental trials are available to obtain requisite information for the proper understanding of this phenomenon. It is on this premise that an attempt is made to conduct a preliminary study to numerically evaluate the buckling of steel columns under eccentric loadings. To achieve this, a static, linear perturbation analysis was initially performed on a pin-ended steel column using the subspace Eigen solver for the different buckled mode shapes to illustrate the likely behaviour of the column when subjected to compressive actions. Then, the static, general analysis was conducted with the column subjected to varying magnitudes of eccentric loadings. It was required to determine the load level at which the column would fail when subjected to these eccentric loadings. Consequently, a base load value equivalent to 10 % of Euler's critical buckling load was used. This load value was thereafter increased by 20 % in sequence. It was discovered that 10 % of the Euler's critical buckling load can alter the stiffness of the column when loaded eccentrically. It was further observed that the steel column finally failed at a load greater than 20 % of the Euler's critical buckling load and 40.1% of Rankine's critical buckling load. This is because the permissible deflection for unbraced columns may be taken as the quotient of effective length of column to 250, which translates to 13.8 mm. Therefore, the maximum deflection of 14.72 mm reached by applying an eccentric load of 514 kN exceeds the allowable limit of 13.8 mm.

1. Introduction

Buckling analysis is essentially required to study the instability problems associated with slender cross sections and thin-walled structural members. It is common knowledge that short and slender columns are extensively utilised in buildings, aircraft construction such as landing gears, mounting legs and so on. Local buckling has been a major concern for structural steel members that are subjected to compressive actions, particularly because they usually comprise thin plates and flanged sections. These structural members may fail in buckling before the section actually attains its overall flexural buckling capacity. However, this phenomenon largely depends on their slenderness ratio,

E-mail address: emmanuelufuah@aauekpoma.edu.ng
https://doi.org/10.37121/jase.v4i1.137

thus reducing the ultimate strength and deformation capacities of the sections. Proper assessment of buckling and post-buckling resistance is paramount in these types of structure. Thermal-mechanical post-buckling analysis of structural elements such as struts and plates have been explicated by various researchers using various methods such as the analytical techniques, the energy methods, the finite difference as well as the finite element methods. The energy methods offer simple procedure for estimating the buckling response variables of the elements of construction. According to Paik and Thayamballi [1], the solutions obtained using the energy methods are not usually conservative, and the accuracy of the results greatly depends on the interpolation functions assumed for the lateral displacement. However, in buckling analysis the energy method provides numerical results that may not exactly represent the actual solutions. However, exact solutions can be realised if the selected displacement functions closely represent the buckling mode shape.

It is well-known that the continual buckling of plates produced by progressive fires can induce irregular tension and compression in the steel plate, which may adversely affect the robustness and integrity of welded joints [2]. The function of the stiffeners in steel-plated constructions is to constrain the plates against out-of-plane deformation. Steel-plated structures will normally fail when the imposed loads exceed the carrying capacity of the plate. Buckling and yielding of structural members occur at different stages of loading. However, different responses and behaviour during loading will be involved until the structure reaches its plastic limit or collapse state. For stiffened plated panels, tripping failure of a stiffener can be caused by an applied bending moment that induces an initial compression in the flange of the stiffener. Tripping is a form of failure found in stiffened plated structures in which the stiffeners rotate about the axis of connection with the plate member. However, Paik and Thayamballi [1] remarked that the torsional capacity of a stiffened panel plays a major role in dictating the tripping behaviour of a stiffener in a stiffened panel. Bailey et al. [3] earlier affirmed that the stiffener's torsional stiffness in comparison with the plate's bending stiffness, to a large extent, controls the failure mode. This type of instability problem may either be caused by imperfections in the plates and stiffeners when subjected to axial compressive actions. Nevertheless, the primary function of the stiffeners is to offer restraints to the lateral deflections in this category of structures when subjected to compressive loadings.

Highly developed structural steels are employed as supporting framework in a vast number of constructions such as cinemas, bridges, sports ground, high rise buildings, stadiums and power plants. In fire design of structures, it is apparent that the probability that these structures can be extremely affected by the assumed maximum accidental loadings is not remote. Such loadings can result from collision, explosion or high-velocity fluid flow that may usually be transient. The occurrence of such event has informed the need for researchers to study the mechanical response of structural steels subjected to increased dynamic loadings. Structural columns in construction are generally susceptible to accidental impact actions, and they are normally found to be critical at the ground level, particularly those situated in busy areas. Topical investigations on damage, failure and collapse of elements of construction have shown that a number of academia and industry-based researchers have directed their research interests towards the study and understanding of the performance of structural members subjected to dynamic impact loading [4].

Generally, the performance of steel structures subjected to fire loadings forms part of the fundamental subject of topical research projects. Deterministic procedures have been traditionally employed to evaluate structural fire design whereby the heat loadings are determined using simple calculation techniques. However, a new method that is able to capture the uncertainties inherent in the heat loads as well as the response parameters of structural members is now widely acceptable within the wider research community. This new method known as the stochastic technique is currently employed by some researchers in the area of risk analysis of structures. However, this new methodology depends more on accurate numerical solutions rather than experimental trials. This development has helped to avoid the huge costs that are essentially associated with experimental programmes.

2. Related Studies

Pagoulatou et al. [5] carried out a numerical investigation to assess the performance of circular concrete-filled double-skin steel

columns subjected to concentric axial loadings in compression. A finite element analysis was implemented in their work to examine the behaviour of these columns. The selection and classification of the appropriate material properties for both the concrete and steel materials was essential to ensure the correct modelling of the double-skin section. Consequently, the authors [5] validated their finite element analysis results with those from previous experimental trials. Based on their investigation, these tubular double-skin columns were assumed to behave like the single-skin columns with enhanced stiffness and reduced weight.

Structural instability problems are rife and efforts to address the fundamental challenge through experimental programmes is further compounded due to unavailability of requisite facilities. A few of the researchers that examined eccentrically loaded compressive members have only attempted to assess the buckling load capacity without much information regarding the deformation capacity. Moreover, it is common knowledge that analytical calculations mostly provide exact solutions with the proviso that the appropriate parameters and methodology are accurately defined. Kruti and Vandynskyi [6] developed a new analytical technique to establish the exact solutions of differential equations for the buckling of columns. They formulated various characteristic equations that were used to determine the buckling coefficients of the columns for different boundary conditions. The authors [6] consequently compared their findings with those obtained using the generalised hyper-geometric function technique and very good agreement was obtained.

Zhang et al. [7] remarked that compression tests of channel column sections having their ends connected by pins and reinforced with bent-up edge stiffeners were not readily available. It is noted that 36 channel sections of different column lengths comprising three different cross sections with varying edge inclined angles acting as stiffeners were tested. The initial geometric imperfections associated with the column sections along with the material properties of the sections were evaluated to ensure accurate prediction of the behaviour. Different failure modes such as local buckling, instability due to flexural effects, torsional instability and the interaction among these failure modes were identified in their tests. Their results signified that the specific points of applied loadings and the bent-up angle stiffeners play a major role in dictating the plastic limit load and collapse mechanism of the specimens.

A wrinkling investigation of sand-wish column members was conducted by Hadi [8] using the finite element method and the classical energy method. In the finite element technique, the Reissner-Mindlin concept was adopted using shell elements to model the material behaviour along the beam thickness. Consideration was given to mesh sensitivity by using very fine shell elements in modelling the outer surface and the hub through the beam thickness. Hadi [8] asserted that for ribbed cores, such buckling problems do not take place, though local buckling of different kinds are likely to develop. The buckling loads were surmised and determined such that the work done by the compressive actions during the lateral deformation induced by the flexural actions of the face layers was made equal to the flexural strain energy stored in the face specimens together with the strain energy of deformation in the core.

James [9] examined buckling problems in columns with adequate consideration given to shear deformation. There are cases where different theories can present very different predictions for a particular column behaviour. The occurrence of shear actions in the column can considerably limit its axial capacity. This may not be a problem for pin-jointed compressive members in view of the fact that they are not designed to resist shear loadings. However, James [9] discovered that the effect of the axial load depends largely on the assumptions made for the direction of the resultant axial load during deformation. This is because during deformation, the resultant axial load may change direction in the deformed configuration thereby altering the calculation process. Therefore, it is surmised that if redistribution of the net axial load is not immediately considered, the solution may be very misleading.

Recently, Kashyap et al. [10] carried out a comparative analysis between theoretical and experimental buckling loads for hollow steel columns. They [10] examined five hollow steel columns having the same length and external diameter with varying wall thicknesses. Their findings show that, for the columns examined, the Euler's model for the buckling load is overly unconservative when compared with experimental values. However, the experimental values were reasonably in good agreement with the values obtained using the Rankine's model. Kashyap et al. [10] further emphasised that the variation in experimental values and those obtained using the Rankine's

model could be due to eccentricities and other related imperfections that are likely during experimental trials. Nevertheless, it was discovered that the variation in the buckling capacity of the column between experimental and Rankine's values with respect to wall thickness was parabolic.

Gupta [11] presented thermal post-buckling investigation of flexible columns by adopting the finite element method and simple analytical technique. The boundary conditions of the columns were such that the ends were axially constrained, and at elevated temperatures greater than the nominal ambient condition of the column, corresponding compressive Thermo-mechanical loads were produced thereby inducing buckling in the column. As the temperature rise above the critical temperature of the specimens, thermal post-buckling phenomenon thereby occurred. As a result of constraints imposed on the axial displacement at the ends of the column, the post-buckling behaviour of the columns was determined by the von-Karman strain-displacement model. Classical and non-classical boundary conditions were considered in the analysis. The findings [11] show that the finite element method and the simple analytical technique were in good agreement.

Sastranegara et al. [12] examined the effect of transverse impact loading on the stability of a column subjected to an axial impact. To do this, an axially loaded column due to impact was subsequently subjected to a transverse impact load thereby limiting the flexural stiffness matrix of the column. The magnification of the post-buckling deformation by the transverse impact facilitated the enhancement of the absorption of the axial impact energy. Furthermore, Sastranegara et al. [12] maintained that the concurrent application of transverse and axial impact loads resulted in the maximum energy absorption. It was discovered that the application of a transverse impact load following an axial impact force on the column showed that the force of transverse impact is likely the governing parameter in the analysis.

Hana et al. [13] conducted tests on square steel tubular frames filled with concrete having varying cross sectional dimensions, breadth to thickness ratio and load applications. It was concluded that the concrete-filled steel tubular frame produced adequate horizontal resistance. It was also suggested that the limiting value of the breadth to thickness ratio of the column can be increased up to 1.5 times that for the unfilled steel tubes. This is probably due to the effects of the concrete found within the core of the steel tube on the local buckling and post buckling performance of the section.

Composite constructions such as steel-concrete composite columns have advantages over steel or concrete columns with regard to its strength and deformation capacities. Ali and Islam [14] assessed the behaviour of different shapes of concrete filled steel tubular (CFST) columns subjected to concentric and eccentric loadings using the correlations described in AISC (2010) guidelines. The different cross sections considered are circular, square, rectangular and elliptical sections. Moreover, the same cross-sectional area of 0.017 m^2 and length of 1.2 m were approximately adopted for the different shapes investigated. The authors [14] discovered that CFST columns of rectangular shape produced the highest axial compressive strength while the elliptical shape produced the lowest value. Nevertheless, Ali and Islam [14] maintained that the circular size CFST columns gave the optimum compressive strength due to its good confinement effects. Particularly interesting is the percentage reduction in the compressive strength of the CFST columns under eccentric loadings. For the different shapes of the CFST columns subjected to eccentric loadings with an eccentricity of 28mm, the percentage reduction in axial capacity is 33% for the square shape, 10% for the circular shape, 34% for the rectangular shape and 23% for the elliptical shape. It is expected that the percentage reduction in the axial compressive strength of a non-composite column under eccentric loadings will be higher due to its lower flexural stiffness.

3. Materials and Methods

3.1. Materials Behaviour of Structural Steels

The stress strain curve of Fig. 1 describes the mechanical properties of steel used in modelling the column. The elastic constant is 200 GPa while the yield value is 460 MPa. Empirical stress and strain data can present different behavioural trends regarding whether they are obtained from the tensile test or compressive test programmes. However, most tests conducted on steels such as those used to determine their yield criteria are obtained from uniaxial tensile test. To account for the variability that may occur, true stress and true strain data are determined

from the nominal or empirical values of these parameters.

True stress-logarithmic strain data for steel have been extensively employed in numerical modelling. In order to obtain the relationship between true stress and true strain it is paramount to normalise the relationship between tensile strain and compressive strain. This can only be achieved with the proviso that within desirable limit the deformation occurring as a result of loading will approach zero. The elemental change in strain may be approximated by the relation of equation (1):

$$d\varepsilon = \frac{dl}{l}. \quad (1)$$

Therefore,

$$\varepsilon_t = \int_{l_0}^{l} \frac{dl}{l} = log_e \frac{l}{l_0}, \quad (2)$$

where, $d\varepsilon$ is the elemental increment in strain, dl is the change in length, l is the new length, l_o is the original length and ε_t is the true or logarithmic strain.

Equation (2) is known as the logarithmic strain. It is related to the nominal strain by the expression given in equation (3). Rearranging the expression of equation (2) yields equation (3):

$$\varepsilon_t = log_e[1 + \varepsilon], \quad (3)$$

where, ε is the nominal (or engineering) strain.

In a similar hypothesis, the true stress can be related to the engineering stress considering the fact that during deformation the mass volume does not change. The expression is thus given in equation (4) as:

$$\sigma_t = \sigma[1 + \varepsilon]. \quad (4)$$

Where, σ_t is the true stress and σ is the nominal (or engineering) stress.

Plastic strain can therefore be extracted using classical theory. One point of fundamental interest is that at first yield, the plastic strain is zero since the plasticity has just begun at this stage of loading.

3.2. Modelling Strategy

The numerical computation was conducted using a general-purpose commercial code-ABAQUS [15], which is able to predict the structural response of elements of construction using the finite element technique. An adequate consideration of the large displacement effects of the finite elements in the non-linear analysis was made using an updated Lagrangian model. The modelling technique includes the solution of the stress-strain behaviour using the Newton-Raphson iterative approach. The bi-linear stress-strain model shown in Fig. 1 describes the inelastic behaviour of the material and the collapse mechanism is determined by the von Mises yield criteria and the associated flow rule [16]. This component of the performance-based design in itself considers the mechanical loading imposed on structures and its effect on structural behaviour. Moreover, Timoshenko and Gere [17] and Wang et al. [18] provide explicit procedure for the derivation of the governing differential equations for the elastic buckling of columns. Therefore, the governing differential equation for the case of constant flexural rigidity is expressed in equation (5).

$$\frac{d^2y}{dx^2} + \frac{P}{EI}y = 0, \quad (5)$$

where, EI is the flexural rigidity and P is the applied load.

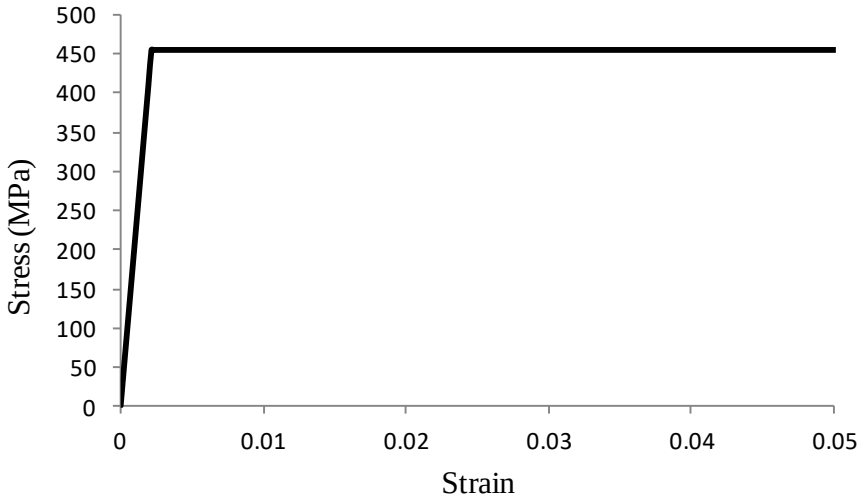

Fig. 1 Stress-strain curve for carbon steel.

Table 1 Geometric properties of the studied column (203x203x46 UC).

Thickness (mm)		Ratios for local buckling		Second moment of area (cm^4)		Radius of gyration (cm)	
Web, t	Flange, T	Web, d/t	Flange, b/T	I_{xx}	I_{yy}	r_x	r_y
7.2	11.0	22.3	9.25	4570	1550	8.82	5.13

Where, UC means universal column, d is the depth between fillets, b is breadth of section, t is web thickness, and T is flange thickness.

The universal column is a 203 x 203 x 46 flanged section having the geometric properties shown in Table 1. The cross-sectional area of the universal column section is 58.7 cm^2. The critical buckling load for the pin-ended column is 2571 kN, which was determined using equation (6). Hence, the critical buckling stress was calculated to be approximately 438 MPa. Fig. 2 shows a typical configuration of loading and boundary conditions of the studied column. The base load was taken as 10 % of the Euler's critical buckling load with a value of approximately 257 kN. This base value was subsequently increased in each calculation step in succession of 20 % increments.

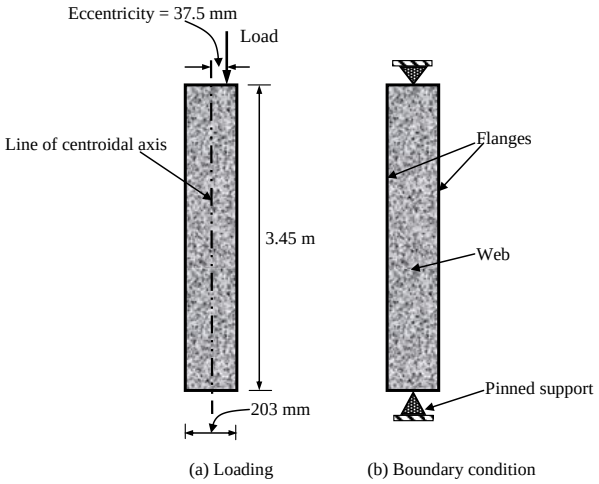

Fig. 2 Two-dimensional representation of loading and boundary conditions of the column

The critical buckling stress derived by dividing the critical buckling load by the cross-sectional area is expressed in equation (7).

$$P_{cr} = \frac{\pi^2 EI}{L^2}. \quad (6)$$

$$\sigma_{cr} = \frac{\pi^2 E}{\left(L/r\right)^2}. \quad (7)$$

Where, P_{cr} is the critical buckling load, σ_{cr} is the critical buckling strength, L is the member length, and r is the radius of gyration.

Conversely, it is assumed that the Euler's correlation of equation (6) is unconservative for short columns when compared with Rankine's model of equation (8). Nonetheless, the choice of Rankine's constant may be very dependent of the material properties adopted. The Rankine's buckling load for the 203x203x46 UC under study is 1282 kN taking the Rankine's constant to be 1/4500. This suggests that the Euler's equation for buckling load may not be suitable for columns with slenderness ratio less than 70. The findings from the study conducted by Kashyap et al. [10] suggest that Euler's model for estimating buckling load may not be suitable for short columns.

$$P_{CR} = \frac{\sigma_c A}{1+a\left(L_e/k_{min}\right)^2}. \quad (8)$$

Where, P_{CR} is Rankine's crippling/buckling load, σ_c is the critical buckling stress, A is cross sectional area, a is the Rankine's constant, L_e is effective length and k_{min} is the minimum radius of gyration.

To verify the numerical tool-Abaqus implemented in the calculation, a scoping study was taken from the literature [10] and analysed. The column is a hollow circular section having the geometric properties and boundary conditions shown in Table 2. The bi-linear stress strain curve of Fig. 3 was used to model the material behaviour of the hollow circular columns using an elastic constant of 210 GPa and a yield strength of 320 MPa.

Table 2 Geometric properties and boundary conditions of the hollow circular columns.

Sample No.	Length (mm)	Wall thickness (mm)	External diameter (mm)	Internal diameter (mm)	Cross section area (mm^2)	Minimum radius of gyration (mm)	Support condition
1	1520	1.6	60	56.8	293.60	20.66	Fixed-ended
2	1520	1.8	60	56.4	329.20	20.59	Fixed-ended
3	1520	2.3	60	55.4	417.00	20.42	Fixed-ended
4	1520	2.9	60	54.2	520.28	20.21	Fixed-ended
5	1520	3.3	60	53.4	587.90	20.08	Fixed-ended

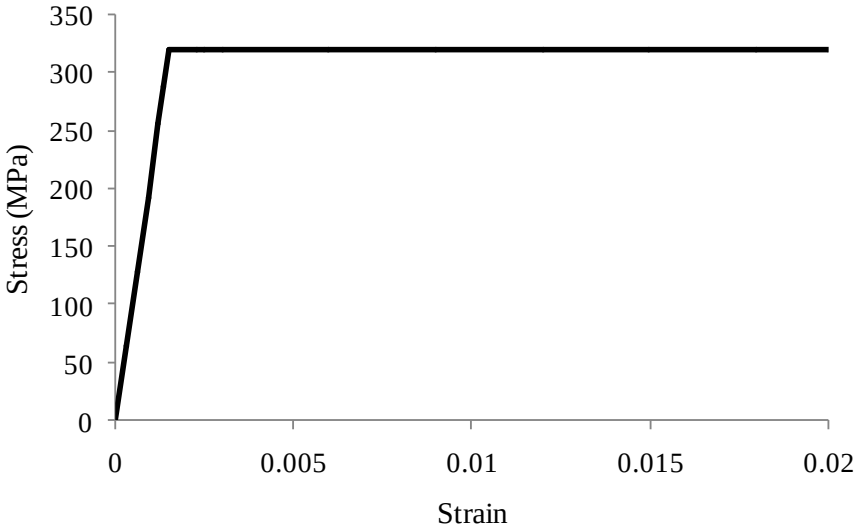

Fig. 3 Stress-strain curve for carbon steel used for the scoping study.

The second order non-linear analysis is assumed to be elastic-perfectly plastic. The equilibrium equation and the corresponding constitutive model used to determine the mechanical strength and behaviour are respectively given in equations (9) and (10) [19]:

$$\sigma_{ij,j} + f_i = 0. \tag{9}$$

$$\{\Delta\sigma\} = \{D^{ep}\}[B]\{\Delta U_e\}. \tag{10}$$

Where, σ_{ij} is a stress tensor, f_i is a body force, Δσ is the incremental stress, D^{ep} is the elasto-plastic stiffness, B is strain-displacement relation and ΔU_e is nodal displacement increment.

The ABAQUS computer code [15] employs the principles of Newton-Raphson to determine the solutions of nonlinear problems. The total load is usually divided into smaller load increments through which approximate solutions, derived from equilibrium consideration are obtained at the end of each load increment. Each increment may contain a number of iterative processes, which continues until the unbalanced force is completely reduced to an acceptable tolerance so that the displacement increment approximates to zero. In ABAQUS [15], the equilibrium for an increment in an analysis step can be achieved when the following condition defined in equation (11) is satisfied.

$$0.005\, q^{\infty} > r^{\infty}_{max}. \tag{11}$$

Where, q^{∞} *is* the time-average force in the structural system and $r^{\infty}_{\max}$ is the maximum force and maximum moment residual points of reference.

To generate the solution to the system of linear algebraic equations denoted by the matrix expression of equation (10), a sequence of linear solver iterations is performed, whereby an approximate solution gets closer to the exact solution at each iterative process. The error in the approximate solution is measured by the residual of the linear system. The approximate solution is said to be converged when the residual is below a specified relative tolerance. However, Abaqus [15] allows a tolerance value of 10^{-6}. Nevertheless, the rate at which the approximate solution converges is directly related to the conditioning of the original system of equations. A linear system that is well conditioned will converge faster than an ill-conditioned system. If the residual does not converge to zero, the iterative solver is said to have stagnated and Abaqus will exit with an error or warning message depending on the magnitude of the final residual. The solution is found by specifying the loading as a function of time to obtain the nonlinear response. Therefore, Abaqus breaks the simulation into a number of time increments, and finds the approximate equilibrium configuration at the end of each time increment. Using the Newton-Raphson's method it often takes Abaqus several iterations to determine an acceptable solution to each time increment. A typical stiffness matrix equation formulated at the local coordinate system is given in equation (12).

$$\begin{bmatrix}\delta F_{11}\\ \delta F_{22}\\ \delta F_{12}\\ \delta M_{11}\\ \delta M_{22}\\ \delta M_{12}\end{bmatrix}=\begin{bmatrix}K_{11} & K_{12} & K_{13} & K_{14} & K_{15} & K_{16}\\ K_{21} & K_{22} & K_{23} & K_{24} & K_{25} & K_{26}\\ \cdots & \cdots & \cdots & \cdots & \cdots & \cdots\\ \cdots & \cdots & \cdots & \cdots & \cdots & \cdots\\ \cdots & \cdots & \cdots & \cdots & \cdots & \cdots\\ K_{61} & K_{62} & K_{63} & K_{64} & K_{65} & K_{66}\end{bmatrix}\begin{bmatrix}\delta u_{11}\\ \delta u_{22}\\ \delta u_{12}\\ \delta \varphi_{11}\\ \delta \varphi_{22}\\ \delta \varphi_{12}\end{bmatrix}. \quad (12)$$

Where, δu_{ij} is an incremental value of the total deformation, $\delta \phi_{ij}$ is an incremental value of the total rotation, δF_{ij} is an incremental value of the total load, δM_{ij} an incremental value of the total moment and K_{ij} is the stiffness matrix.

The variation in stiffness beyond the elastic regime necessitates iterative means in the calculation procedure. As earlier mentioned, Abaqus [15] adopts the Newton-Raphson's technique to incrementally solve the resulting differential equations. After measuring the released strains, the stresses can then be calculated. It can be surmised that the force-displacement model of equation (13) is equivalent in behaviour to that of equations (10) and (12).

$$Q_i = K_{ij}u_j. \quad (13)$$

Where, Q_i is the force or stress resultant in the local coordinate system, K_{ij} is the stiffness matrix and u_j is the displacement component in the local coordinate system.

Suppose we represent the transformation matrix in the local coordinate system as β, we have a relationship between the force components in the local and global coordinate systems as given in equation (14):

$$Q_i = \beta F_i. \quad (14)$$

To transform from the global to the local coordinate system, equation (14) is implemented. The transformation from local to global coordinate system can be performed by using equation (15).

$$F_i = \beta^T Q_i. \quad (15)$$

Where, F_i is the force component in the global coordinate system and β^T is the transpose of the transformation matrix in the local coordinate system.

The stiffness matrix relation in the global coordinate system can therefore be derived as given in equation (16):

$$F = \beta^T Q = \beta^T K u. \quad (16)$$

But $u = \beta v$, where v represents the displacement component in the global coordinate system.

Therefore, the transformation from local to global coordinate system can be determined with the correlation of equation (17):

$$F = \beta^T K \beta v. \quad (17)$$

Where, $\beta^T K \beta$ is the member stiffness matrix in the global coordinate system.

3.3. Cross-Section Capacity and Buckling Resistance Verification

The column is subjected to a maximum axial load of 514 kN and uniaxial bending moment of 19.275 kNm. With a flange thickness of 11.0 mm, the design strength of the column is 460 N/mm^2. According to BS 5950, Part 1 [20], for Class 1 (Plastic) section, the limiting ratio for local web buckling is given by equation (18).

$$d/t < \frac{80\,\varepsilon}{1+r_1}, \quad (18)$$

where $r_1 = \frac{F_c}{dtp_y}$, but $-1 \le r_1 \le 1$; F_C is the Axial compression load, d is the depth between fillets, t is the web thickness, p_y is the design strength, and $\varepsilon = \sqrt{275/p_y}$.

It is noted that the flange is not plastic. However, the limiting ratio for local flange buckling for Class 3 (Semi-compact) section is expressed in equation (19):

$$b/T < 15\varepsilon. \quad (19)$$

The result of section classification for the column is illustrated in Table 3 whereby the flange is semi-compact and the web is plastic. To verify strength and deformation capacities of the section, equations (20) and (21) were carefully implemented to assess the section capacity and buckling check respectively [20].

$$\frac{F_C}{A_g p_y} + \frac{m_x M_x}{M_{Cx}} + \frac{m_y M_y}{M_{Cy}} < 1. \quad (20)$$

Table 3 Section classification for the 203x203x46 UC.

$r_1 = \frac{514000}{160.8x7.2x460} = 0.965$	Actual ratios for local buckling		Limiting ratios for local buckling	
	Web, d/t	Flange, b/T	Web, d/t	Flange, b/T
	22.3	9.25	31.47	11.56

$$\frac{F_C}{P_C}+\frac{m_x M_x}{p_y Z_x}+\frac{m_y M_y}{p_y Z_y}<1. \quad (21)$$

Where, m_x, m_y are the equivalent moment factors for flexural buckling, M_{cx}, M_{cy} are the moment capacities about the major and minor axes respectively, M_x, M_y are the induced/ applied moment about the major and minor axes respectively, Z_x, Z_y are the elastic section moduli about the major and minor axes respectively and A_g is the gross sectional area of the section.

For the uniaxial loading, the moment about the minor axis, M_y was taken as zero whereas the equivalent moment factors were assumed as follows: $m_x = m_y = 1$. Hence, for the semi-compact section, equation (20) becomes:

$$\frac{514000}{58.7\times100\times460}+\frac{1x19.275}{207}=0.283<1.$$

The slenderness ratio of the column is 67.25 with the corresponding compressive strength, p_c = 297 N/mm^2. The compressive capacity, $P_c = A_g\, p_c$ = 58.7 x 10^2 x 297 = 1743.4 kN.

Therefore, equation (21) becomes:

$$\frac{514}{1743.4}+\frac{1x19.275}{460\times450\times10^{-3}}=0.388<1.$$

Therefore, the section capacity and buckling strength are satisfactory.

Generally, Abaqus has a list of interpolation functions and their corresponding shape functions defined within the element library [15]. Abaqus selects a displacement function appropriate for a given analysis. The corresponding shape functions are then identified by the elements throughout the iterative process. Moreover, the likely displacement function adopted in this calculation and the corresponding shape function are given in equations (22) and (23) respectively, as:

$$f(x)=A\sin\lambda x+B\cos\lambda x, \quad (22)$$

$$\lambda=\sqrt{P/EI}, \quad (23)$$

where, *f(x)* is the displacement function, *A* and *B* are arbitrary constants, λ is the Eigen value representing the shape function, *P* is the compressive load, *E* is elastic constant and *I* represents the second moment of area.

3.4. Mesh Sensitivity Analysis

The 4-node quadratic shell elements, S4R were used to model the column under investigation. To capture the nonlinear response associated with the inelastic behaviour, five section points were specified through the element thickness where numerical integration was implemented to evaluate the response at each section point. These shell elements have three translational and three rotational degrees of freedom. Mesh sensitivity study was conducted to ensure that the actual nonlinear behaviour was captured. It is however noted that most quadratic shell elements are not very sensitive to mesh refinements because there are no shear or membrane locking problems associated with them.

4. Results and Discussion

The matrix of mesh sensitivity study showing the effect of mesh refinements is presented in Table 4 and Fig. 4. It is apparent from Fig. 4 that the 4-node quadratic shell elements, S4R are not very sensitive to mesh refinement. However, to avert convergence problem in the calculation process, the stress strain curve was defined such that no negative stiffness matrix is possible in the computation process. The adoption of the bilinear stress strain curves of Figs. 1 and 3 ensures that a positive stiffness matrix is maintained throughout the calculation step. It is noted that the 4-node quadratic shell elements have the capability of eliminating the occurrence of hourglass stiffness [15].

Table 4 Applied eccentric loads and the resulting lateral deflections for the column.

Applied load (kN)	Mid-span displacements (mm)			
257	1.63	1.46	1.39	1.39
308	2.52	2.26	2.15	2.15
360	4.03	3.61	3.44	3.44
411	6.78	6.08	5.79	5.79
463	11.49	10.31	9.82	9.82
514	17.24	15.46	14.72	14.72
Element size	5x86	10x172	20x345	25x425
No. of elements	1290	5160	20700	31838

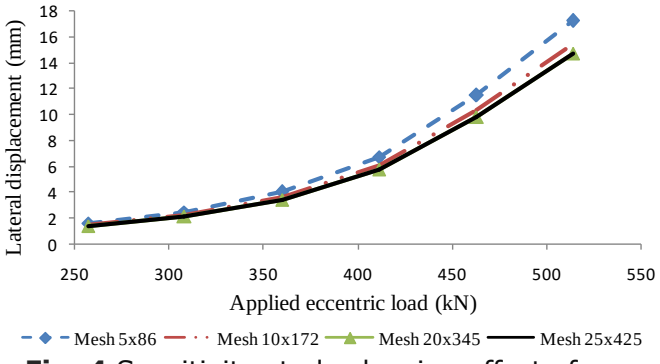

Fig. 4 Sensitivity study showing effect of mesh refinement.

Table 5 Buckling loads comparison obtained in the scoping study.

Wall thickness (mm)	Experimental Crippling Load (kN)	Rankine's Crippling Load (kN)	Abaqus Crippling Load (kN)	Euler's Crippling Load (kN)
1.6	58.84	79.53	72.43	425.02
1.8	73.55	88.26	84.98	473.37
2.3	112.78	109.83	110.09	589.77
2.9	144.16	140.24	136.70	731.97
3.3	176.52	157.89	162.54	804.15

Moreover, the results from the scoping study are presented in Table 5 and Fig. 5. A reasonable agreement is attained in comparison with the experimental values. Kashyap et al. [10] calculated the Euler's buckling load shown in Table 4. However, considering Fig. 6, it is apparent that the crippling load determined by Euler's model according to Kashyap et al. [10] is not appropriate for short columns. Therefore, the buckling load calculated by Euler's model may be seen to have been over-estimated for the column in this study.

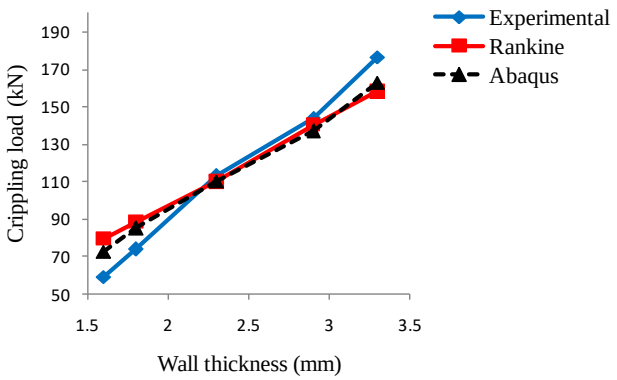

Fig. 5 Buckling loads comparison for the scoping study.

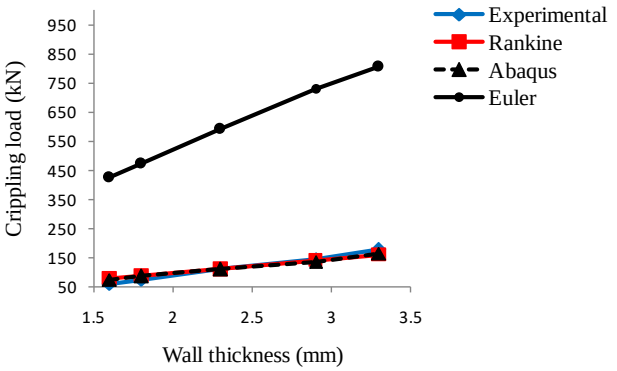

Fig. 6 Buckling loads comparison including Euler's crippling load.

The slenderness ratio for the 203x203x46 universal column (UC) of length 3.45 m was therefore computed to be 67.25. Based on the computational strategy, the buckling strength was plotted against the non-dimensional slenderness ratio shown in Fig. 7. It is apparent from Fig. 7 that up to the critical slenderness ratio of 67.25, the buckling strength of the pin-ended column remained unchanged. It is expected that the reduction in the buckling strength of the column will begin as the slenderness ratio becomes larger than 67.25. However, it is noted that the buckling strength of a column is inversely proportional to the square of the slenderness ratio as revealed in Fig. 7.

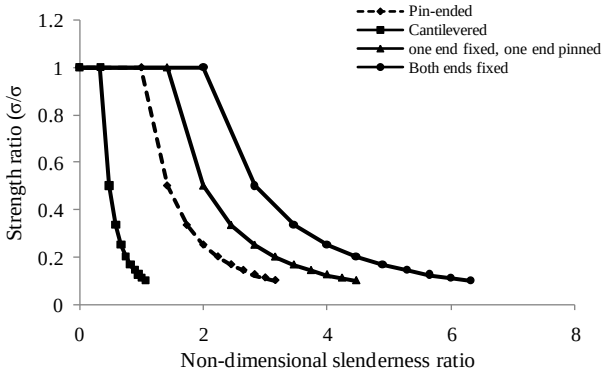

Fig. 7 Buckling strength curves for the 203x203x46 UC with various end conditions.

The analysis of column subjected to varying compressive loadings with an eccentricity of 37.5 mm was performed to evaluate the structural behaviour of the element under eccentric loadings. The critical buckling load for the column was determined using both the Euler's model and the Rankine's model. Under concentric loadings, the column is able to sustain the appropriate load. However, when subjected to eccentric loadings secondary stresses are further induced in the column due to bending. To study this phenomenon, 10 % of the Euler's critical buckling load was used as the initial load for the calculation. Subsequent computations were conducted by increasing the base load in sequence of 20 % increments. It is shown in Fig. 8 that a load of 257 kN and a moment of 9.6375 kNm can induce a maximum lateral displacement of 1.39 mm with an eccentricity of 37.5 mm for the laterally unbraced 203x203x46 UC. As the load is further increased by 51 kN, the resultant mid-span displacement becomes

2.15 mm. Consequently, by subjecting the column to an eccentric load of 514 kN and a bending moment of 19.275 kNm, the resultant lateral displacement was 14.72 mm. The trend in deflection as additional loads of 51 kN are added appears to be nonlinear. Findings show that the maximum applied load of 514 kN representing 20% of Euler's crippling load and 40.1 % of Rankine's crippling load can initiate a geometric failure in the unbraced column at an eccentricity of 37.5 mm. However, the slenderness of the column is an important consideration in this regard. The buckled shapes of the column are presented in Fig. 9.

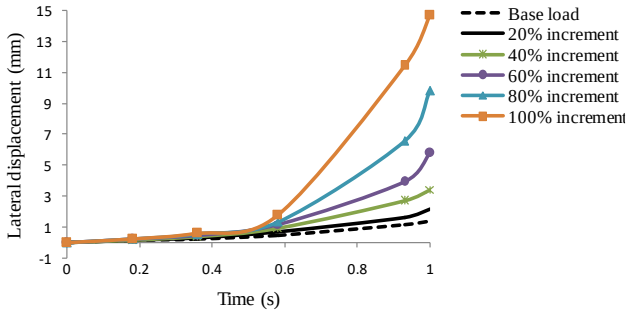

Fig. 8 Lateral displacement-time histories of the 203x203x46 UC.

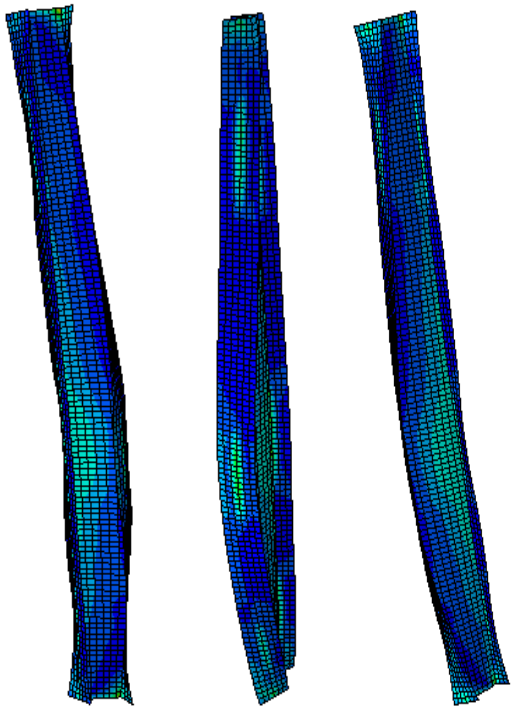

Fig. 9 Overall buckling shapes of the column under loading.

5. Conclusion

The occurrence of structural collapse in buildings can be very detrimental both to personnel and installations. Some of these failures are caused by inadvertent oversights during construction while others can be due to poor craftsmanship. Findings from the numerical study show that eccentric loads of 20% of Euler's critical buckling load and 40.1% of Rankine's critical buckling load with an eccentricity of 37.5 mm can induce a geometric failure of a typical 203x203x46 universal column. It has been demonstrated that beyond the critical slenderness ratio of flanged column sections, buckling strength of the steel columns begins to decrease for the case of pin-ended columns. It is also noted that buckling of the section is governed by the smallest second moment of area and the magnitude of the buckling load is a function of the boundary conditions. In the case of the cantilever as revealed in the analysis for various end conditions, the column's buckling strength begins to decrease before reaching the critical slenderness ratio. Generally, as the end conditions become more rigid, the critical buckling strength is retained up to 1.4 times the critical slenderness ratio for the one end pinned, one end fixed case and 2 times the critical slenderness ratio for the case of fixed ended column as demonstrated in buckling strength curves analysis.

Conflict of Interests

The author declares that there is no conflict of interests regarding the publication of this paper.

ORCID

E. Ufuah https://orcid.org/0000-0002-1010-6218

References

[1] P. K. Paik, and A. K. Thayamballi, *Ultimate limit State Design of Steel-Plated Structures*, West Sussex: John Wiley & Sons, 2002, pp. 13-15.

[2] E. Ufuah, and C. G. Bailey, "Performance of offshore platform deck under running pool fire," 6th European Conference on Steel and Composite Structures, European Convention for Constructional Steelwork, August 31 - September 2, Budapest, Hungary, 2011, pp. 1635-1640.

[3] C. G. Bailey, I. W. Burgess, and R. J. Plank, "The lateral-torsional buckling of unrestrained steel beams in fire," *J. Constr. Steel Res.*, vol. 36, no. 2, pp. 101-119, 1996.

[4] S. M. Fadi, and A. Farid, "Nonlinear finite element modelling of dynamic localizations in high strength steel columns under impact," *Int. J. Impact Eng.*, vol. 52, pp. 47-61, 2013.

[5] M. T. Pagoulatou, X. H. Dai, and D. Lam, "Finite element analysis on the capacity of circular concrete-filled double-skin steel

tubular (CFDST) stub columns," *Eng. Struct. J.*, vol. 72, pp. 102–112, 2014.
[6] Y. Kruti, and V. Vandynskyi, "Exact solutions of buckling problem of columns loaded by self-weight," *Conf. Ser.: Mater. Sci. Eng*., 708012062, 2019.
[7] Y. Zhang, C. Wang, and Z. Zhang, "Tests and finite element analysis of pin-ended channel columns with inclined simple edge stiffeners", *J. Constr. Steel Res*., vol. 63, pp. 383-395, 2007.
[8] B. K. Hadi, "Wrinkling of sand wish column: comparison between finite element analysis and analytical solution", *Composite Structure*, vol. 53, pp. 477- 482, 2001.
[9] M. K. James, "Shear deformation and buckling of columns revisited," *Civ. Eng. Res. J.*, vol. 2, no. 1, pp. 14-18, 2017.
[10] S. K. Kashyap, S. Kumar, M. Mallick, R. P. Singh, and M. Verma, "A comparative study between experimental and theoretical buckling load for hollow steel columns," *Int. J. Eng. Sci. Tech*., vol. 10, no. 3, pp. 27-33, 2018.
[11] R. K. Gupta, "Comparative study of thermal post-buckling analysis of uniform slender and shear flexible columns using rigorous finite element and intuitive formulations," *Int. J. Mech. Sci*., vol. 51, pp. 204–212, 2009.
[12] A. Sastranegara, T. Adachi, and A. Yamaji, "Improving energy absorption of impacted column due to transverse impact: a finite element analysis," *Int. J. Impact Eng*., vol. 32, pp. 444–460, 2005.
[13] L-H. Hana, W-D. Wang, and X-L. Zhao, "Behaviour of steel beam to concrete-filled SHS column frames: finite element model and verifications," *Eng. Struct*., vol. 30, pp. 1647-1658, 2008.
[14] R. B. Ali, and M. M. Islam, "Concentric vs. eccentric loadings on different shapes of CFST columns: a theoretical investigation on axial compressive strength according to AISC guidelines," *World Sci. News*, vol. 99, pp. 119-132, 2018.
[15] ABAQUS Standard/explicit user's manual, Version 6.8-2, vol. 1,2,3 and 4. USA: Dassault Systèmes Simulia Corp., Providence, RI.
[16] P. M. M. Vila Real, N. Lopes, L. Simões da Silva, P. Piloto, and J. M. Franssen, "Numerical modelling of steel beam-columns in case of fire-comparison with Eurocode 3," *Fire Saf. J.*, vol. 39, pp. 23-39, 2004.
[17] S. P. Timoshenko, and J. M. Gere, *Theory of Elastic Stability*, New York: McGraw Hill, 1961.
[18] C. M. Wang, C. Y. Wang, and J. N. Reddy, *Exact Solutions for Buckling of Structural Members*, Florida: CRC Press LLC, 2005.
[19] E. Ufuah, and H. T. Tashok, "Behaviour of stiffened plates subjected to accidental loadings," *Eng. Lett*., vol. 21, no. 2, pp. 95-100, 2013.
[20] BS 5950: Part 1, Structural use of steelwork in buildings; Code of practice for design-rolled and welded sections, 2000.